Новости с конференции "The galaxy life-cycle From activity to quiescence, and back, across cosmic times" и обзор astro-ph

Егорова Е.С.

09.11.2016

Доклад Claude Carignan «Observational evidences of inflow and outflow from HI observations of nearby galaxies»

HVC:

- В Млечном Пути
- M101 — van der Hulst & Sancisi, 1988
- NGC2403 — Fraternali et al 2002, de Blok 2014
- NGC891
- NGC6946 — Boomsma et al 2008

Космологический филамент, соединяющий (и подпитывающий) M31 и M33?
Braun, Thikler, 2004
Wolfe et al, 2016

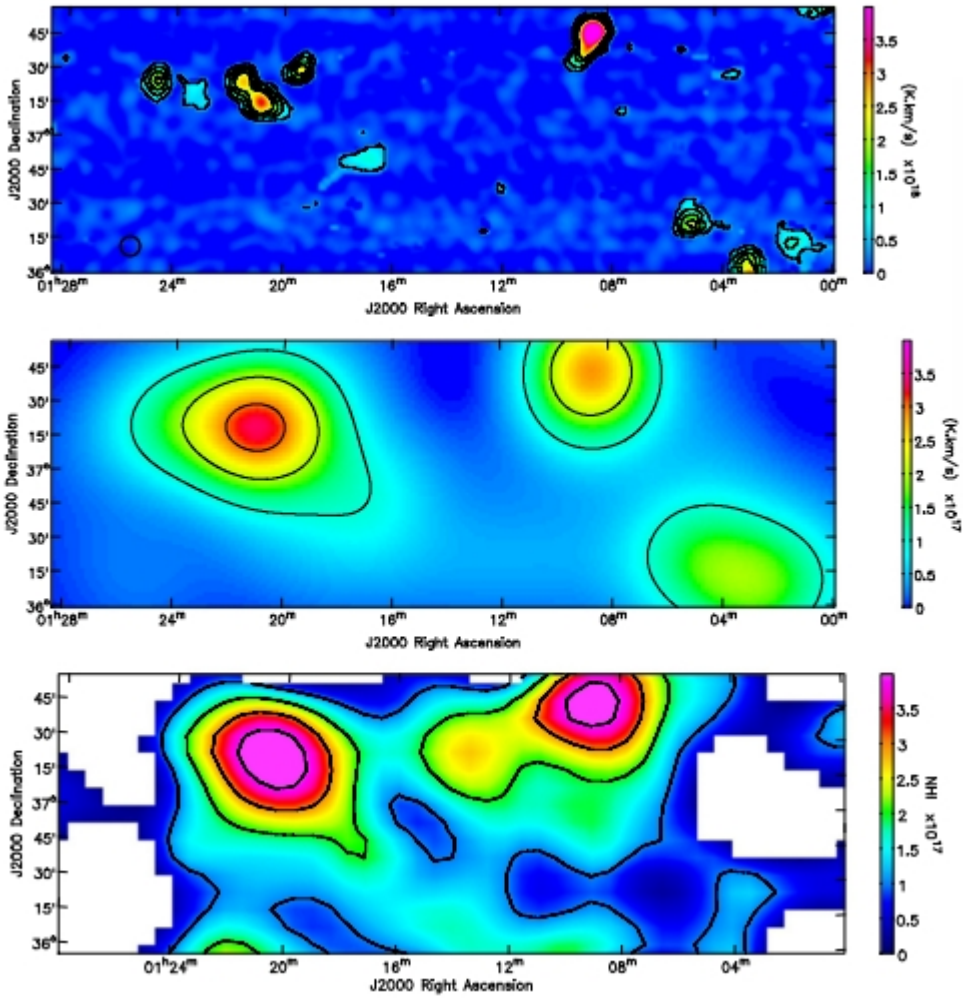

Важна не только чувствительность, но и разрешение!

Но есть прогресс!
Kat-7, Южная Африка, 7*12м. С декабря 2010г.

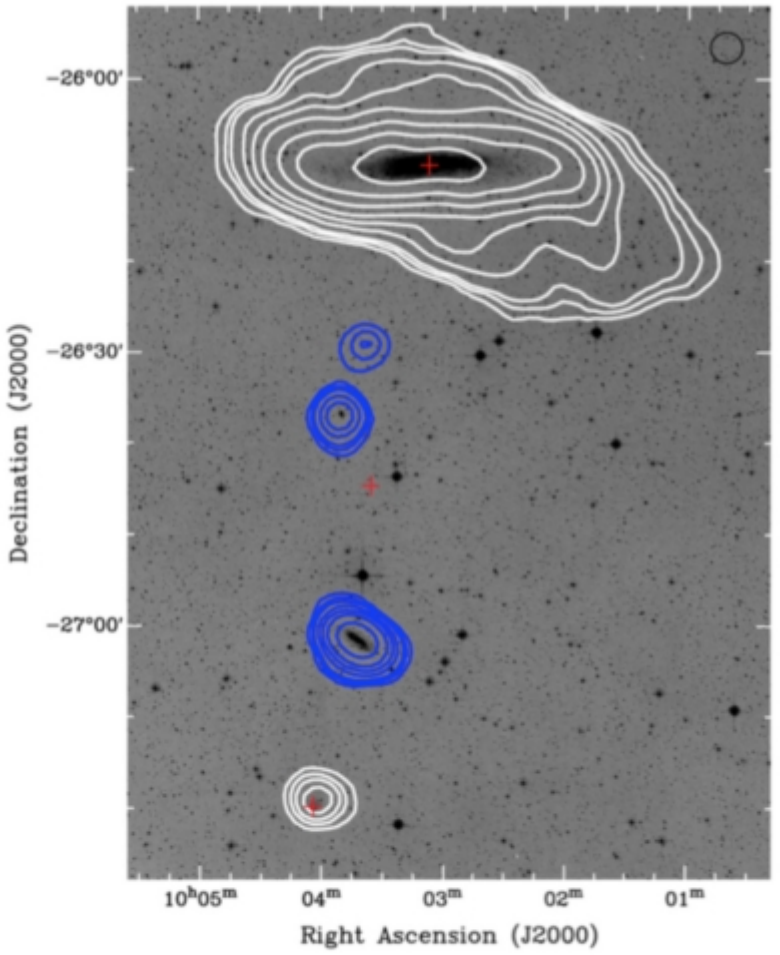

Figure 3. HI distribution of NGC 3109 (top) and of the Antlia dwarf (bottom). The blue countours are background galaxies.

NGC 3109: Кривая вращения — в 2 раза дальше, чем из предыдущих наблюдений. Оцененная масса HI на ~40% выше, чем по данным VLA

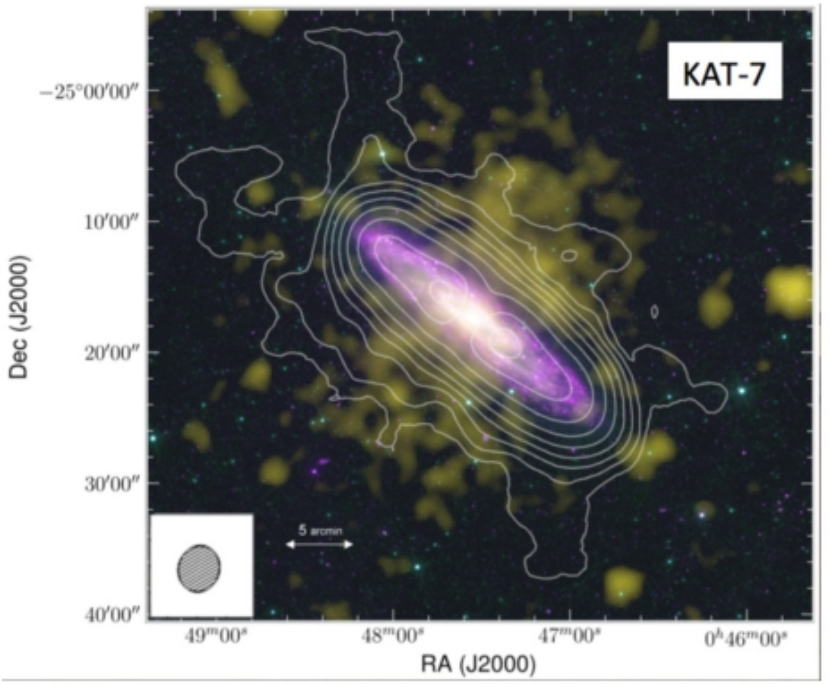

Figure 4. HI distribution of NGC 253 (countours) superposed on a WISE image. The X-ray emission is in yellow.

NGC 253: Поток на 33% больше, чем по данным VLA. В основном за счет внешних областей и гало.
Кинематика газа вне диска указывает на то, что имеет место отток газа и галактический фонтан.

Дальше будет еще лучше!

MeerKAT. 64*13.5м, максимальная база 8км. Конец 2017 года
→ MHONGOOSE 30 галактик по 200 часов

Дальше - SKA

Table 1. Expected sensitivities of different telescopes at 5σ.

Telescope Array(s)	Integration hours	resolution km s^{-1}	beam arcsecs	sensitivity cm^{-2}	Expected date
VLA (THINGS)	10	5	30	5.0×10^{19}	
KAT-7	100	5	210	5.0×10^{18}	
WSRT (HALOGAS)	120	5	30	5.0×10^{18}	
KAT-7 + WSRT	100	16	210	1.0×10^{18}	
MeerKAT	200	16	90	5.0×10^{17}	2017
SKA_1-MID	100	5	30	7.5×10^{17}	2023
SKA_2	10	5	30	2.5×10^{17}	2030
SKA_2	100	5	30	7.5×10^{16}	2030

Carignan 2016:

However, in the near future (2017), the best combination to study low column density HI with a good spatial resolution will be to combine the sensitivity of FAST with the spatial resolution of MeerKAT. The combination of the data from those two telescopes will allow, 6 years before SKA_1-MID, to do "cosmic web" research to levels $< 5.0 \times 10^{17}$ cm^{-2}, close to 10^{16} cm^{-2}, densities that would normally only be accessible to the full SKA around 2030. It is at those densities that we expect the galaxies to connect with the surrounding cosmic web.

UGC 3672: An unusual merging triplet of gas-rich galaxies in the Lynx-Cancer void

J.N. Chengalur,[1⋆] S.A. Pustilnik,[2†] E.S. Egorova[3]

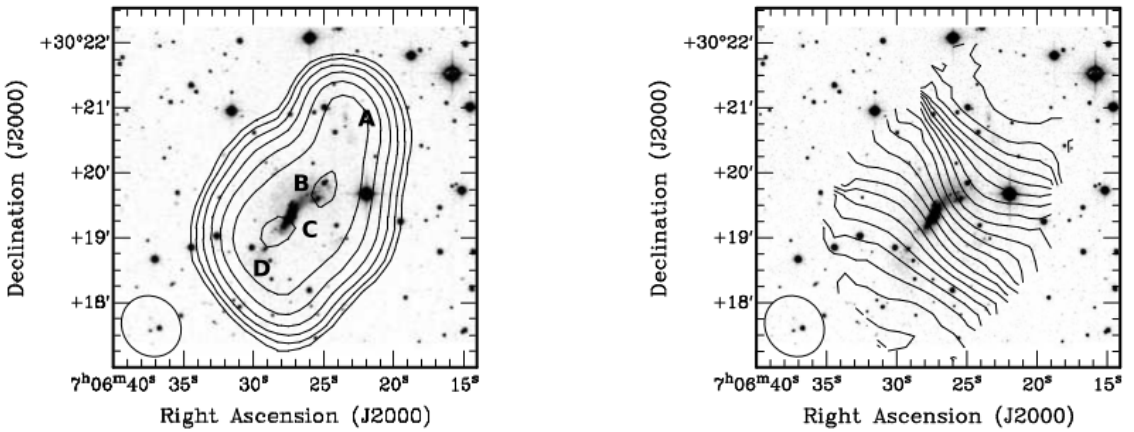

Figure 1. Left Panel: An overlay of the integrated HI emission (contours) at a resolution of $58\farcs5 \times 52\farcs6$ on a KPNO 0.9m B band optical image (greyscales) of the UGC 3672 system. The HI contours start at a column density of 5.5×10^{19} atoms/cm^{-2} and are spaced a factor of 1.5 apart. See the text for the labelling of the different components. The beam is shown in the bottom left. **Right Panel:** Velocity field obtained from the HI data cube (the first moment map). The spatial resolution is $58\farcs5 \times 52\farcs6$. The velocity contours go from 929 km s^{-1} to 1040 km s^{-1} in steps of 5 km s^{-1}. A smooth velocity gradient, consistent with that expected from rotation is seen across the entire system.

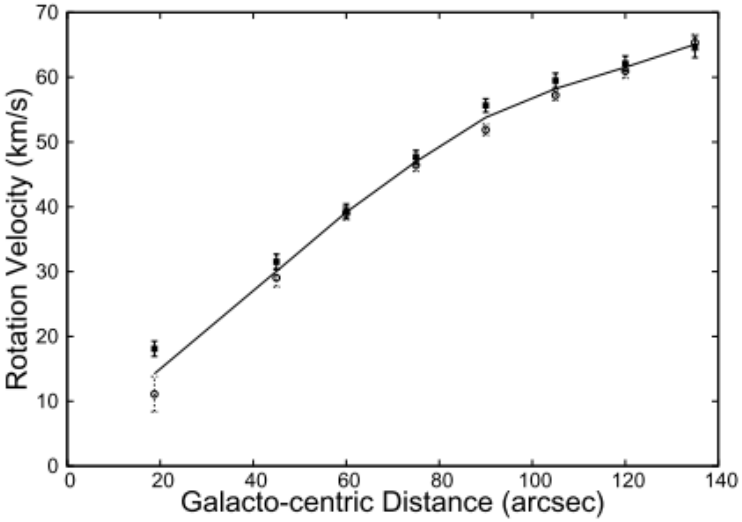

Figure 3. The rotation curve for UGC 3672, derived using the GIPSY program rotcur from the velocity field at a resolution of $58\farcs5 \times 52\farcs6$. The points with the error bars show the rotation curve as derived for the approaching and receding sides separately, while the solid line shows the rotation curve derived using the entire galaxy. There is reasonably good agreement between the rotation curves derived from the two halves separately.

Распределение и кинематика HI — вполне типичны для карликовой иррегулярной галактики

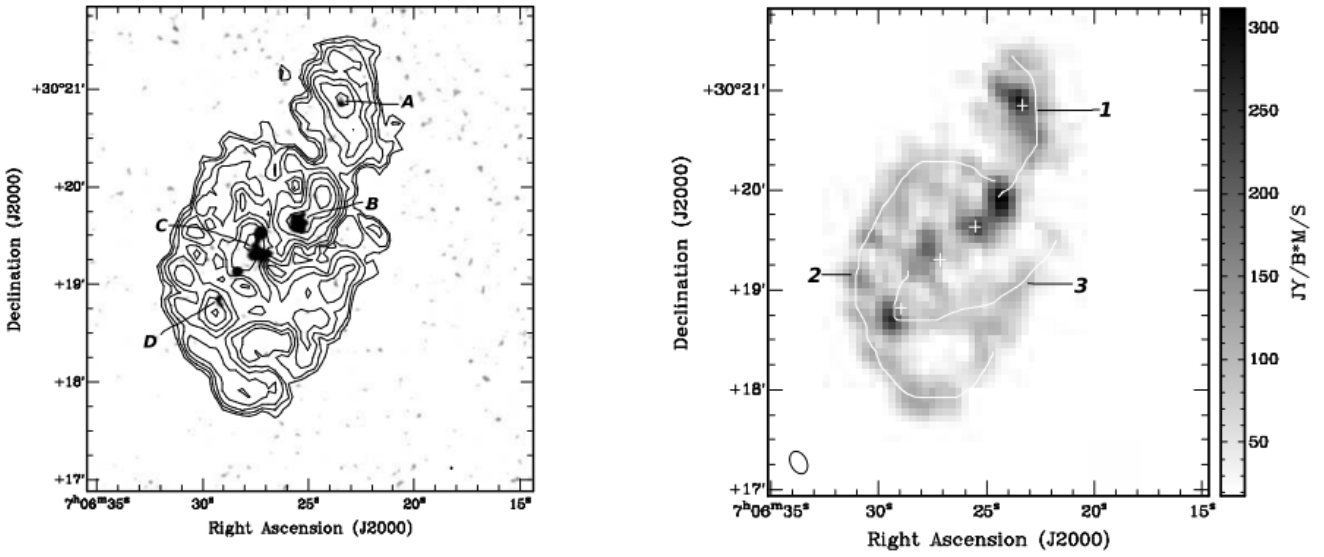

UGC3672 - результат мерджера комп. B и C. Компонент D — на пересечении двух приливных хвостов. Компонент A — отдельная галактика (UGC3672A).

Figure 4. Left: The HI emission from the UGC 3672 system at a resolution of 14.″6 × 10.″1 (contours) overlaid on the Hα emission (greyscales). The Hα data is from van Zee (2000), and has been smoothed to a resolution of 3″. The HI contours start at 1.7 × 10^{20} atoms/cm^{-2} and increase in steps of $\sqrt{2}$. **Right:** Greyscale representation of the HI emission at a resolution of 14.″6 × 10.″1. The beam size is shown in the lower left corner. The locations of the components A to D (going from north to south) are marked by crosses. Three filamentary structures (1,2,3) are also marked. As discussed in the text, the velocity varies continuously along these filaments.

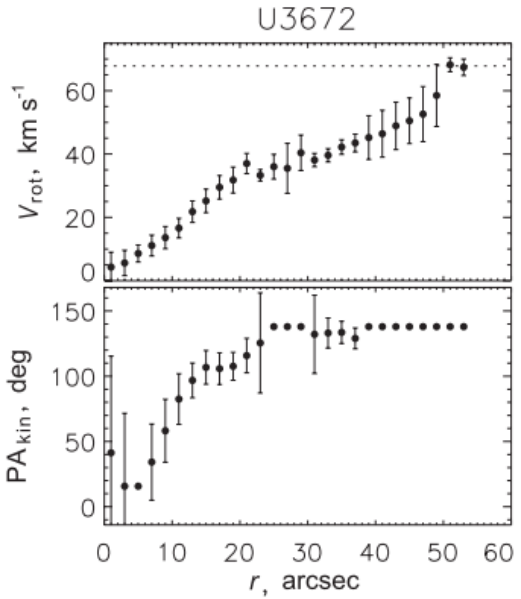

А.Моисеев, 2014:
… Наблюдаемая картина нестационарна, является результатом приливного воздействия или захвата материи разрушенного компаньона. Возможно, что это полярная структура в процессе формирования.

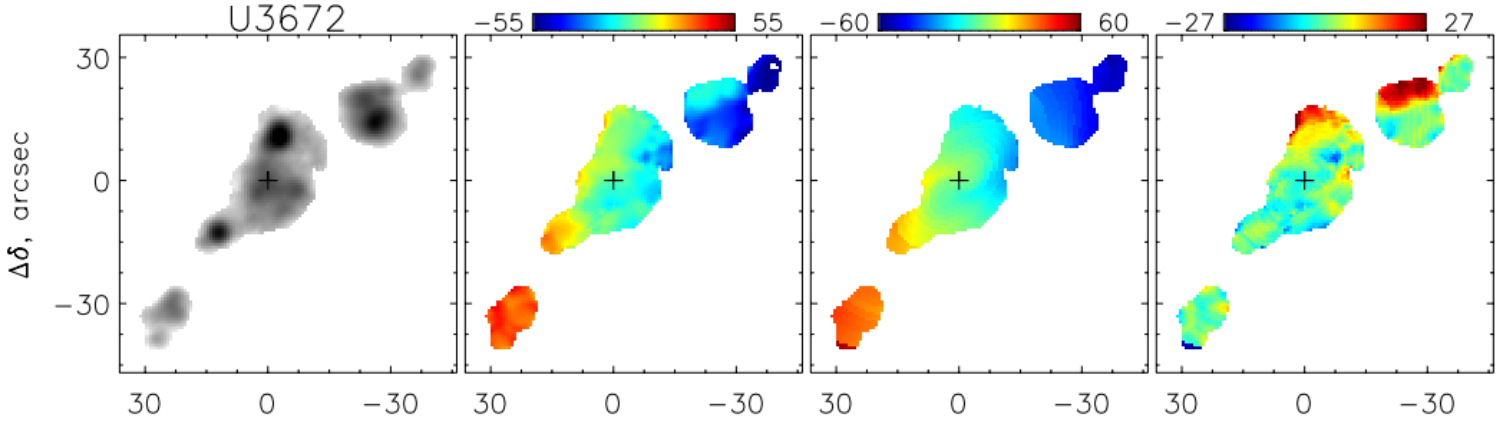

Численное моделирование показывает, что в случае богатых газом дисков в результате слияний могут образовываться дисковые системы. Однако это также зависит от того, доминирует ли в диске clumpy turbulent gas. Считается, что начиная с z~1-2 доминирует, и в этом случае дисковая система не образуется.

UGC 3672A
M_HI/L_B~17
12+logO/H~7.0

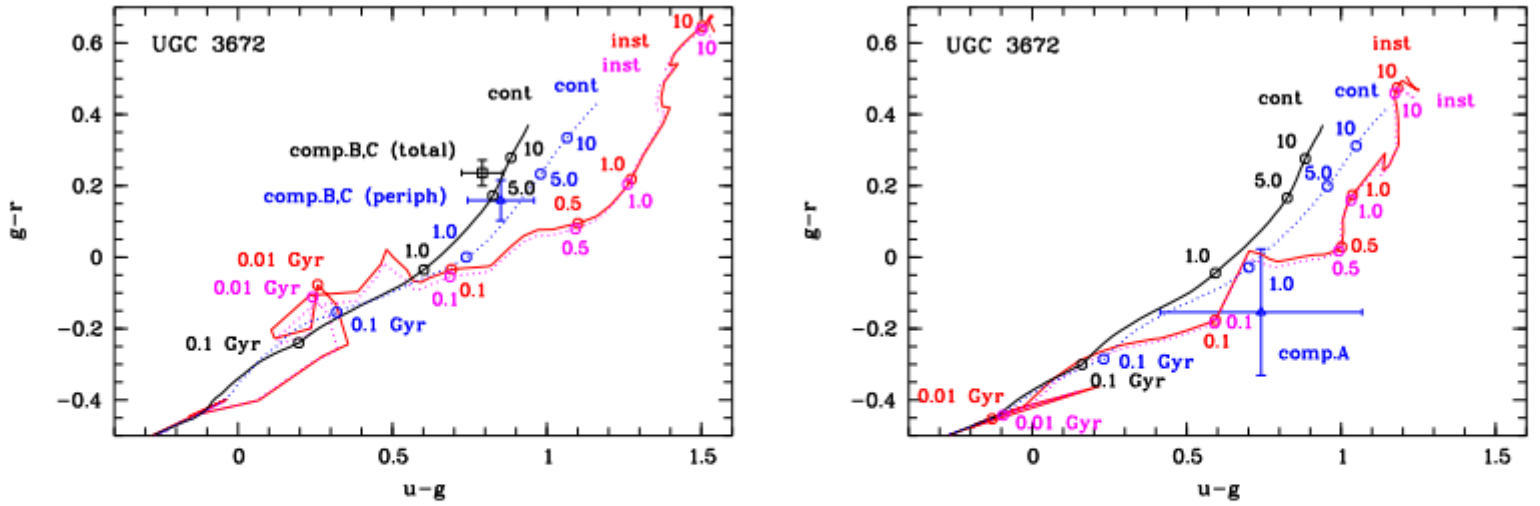

Figure 8. Extinction-corrected colours $g-r$ vs $u-g$ with their $\pm 1\sigma$ uncertainties as measured on the SDSS DR12 images. **Left panel:** blue triangle - for outer parts of combined components B and C, black square - colours of B and C integrated light. **Right panel:** for the total light of component A. They are overlaid on the PEGASE2 package evolutionary tracks from Fioc & Rocca-Volmerange (1999) with tickmarks in Gyr. Both tracks for continuous SF law with constant SFR (*cont*) and the instantaneous starburst (*inst*) are shown as extreme options. See more details in the text. For components B and C the metallicity of tracks is $z = 0.004$, close to that of HII regions with 12+log(O/H) ~8.0. For component A we adopt the metallicity of tracks $z = 0.0004$, corresponding to its tentative gas metallicity of 12+log(O/H)=7.0 from Pustilnik, Perepelitsyna & Kniazev (2016, MNRAS, submitted).

The growth of the central region by acquisition of counter-rotating gas in star-forming galaxies

Yan-Mei Chen[1,2,3,*], Yong Shi[1,2,3], Christy A. Tremonti[4], Matt Bershady[4], Michael Merrifield[5], Eric Emsellem[6,7], Yi-Fei Jin[1,2,3], Song Huang[8], Hai Fu[9], David A. Wake[10], Kevin Bundy[8], David Stark[8], Lihwai Lin[11], Maria Argudo-Fernandez[12,13], Thaisa Storchi Bergmann[14,15], Dmitry Bizyaev[16,17], Joel Brownstein[18], Martin Bureau[19], John Chisholm[4], Niv Drory[20], Qi Guo[21], Lei Hao[12], Jian Hu[22,23], Cheng Li[22,23], Ran Li[21], Alexandre Roman Lopes[24], Kai-Ke Pan[16], Rogemar A. Riffel[15,25], Daniel Thomas[26], Lan Wang[21], Kyle Westfall[26], Ren-Bin Yan[27]

Abstract

Galaxies grow through both internal and external processes. In about 10% of nearby red galaxies with little star formation, gas and stars are counter-rotating, demonstrating the importance of external gas acquisition in these galaxies. However, systematic studies of such phenomena in blue, star-forming galaxies are rare, leaving uncertain the role of external gas acquisition in driving evolution of blue galaxies. Based on new measurements with integral field spectroscopy of a large representative galaxy sample, we find an appreciable fraction of counter-rotators among blue galaxies (9 out of 489 galaxies). The central regions of blue counter-rotators show younger stellar populations and more intense, ongoing star formation than their outer parts, indicating ongoing growth of the central regions. The result offers observational evidence that the acquisition of external gas in blue galaxies is possible; the interaction with pre-existing gas funnels the gas into nuclear regions (< 1 kpc) to form new stars.

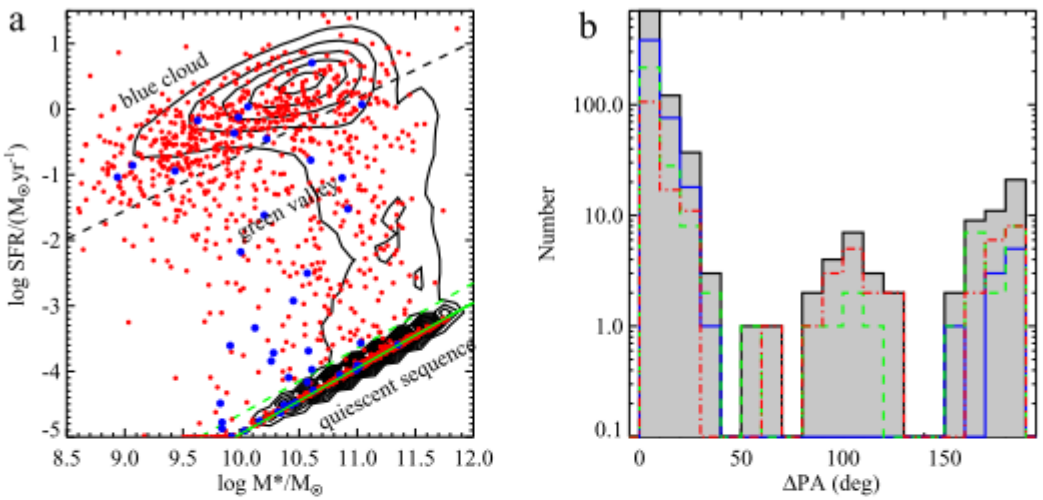

Figure 2: **SFRs versus stellar masses and ΔPA distribution.** (a) SFRs vs. stellar mass. Contours show the SDSS DR7 sample, while the red dots are MaNGA galaxies. The blue dots are the counter-rotators with $\Delta\mathrm{PA} > 150°$. The two dashed lines separate the galaxies into blue star-formers, green valley, and red quiescent galaxies. The black dashed line is adopted from Fig. 11 of *ref*.[18] as an approximation of the boundary (at the 1σ level in scatter) of the star-forming main sequence. The green solid line with log sSFR ($\equiv \mathrm{SFR}/M_*$) ~ -15 remarks red galaxies in which the SFR can be neglected. The region between the black and green dashed lines is referred as the green valley. Although galaxies in the green valley have low SFR, they are clearly distinguished from red galaxies. We do not use the color-magnitude diagram to separate blue from green and red galaxies since the colors are strongly effected by dust extinction. (b) ΔPA distribution for MaNGA galaxies with nebular emission. The grey histogram is for the whole sample, red for the red quiescent galaxies.

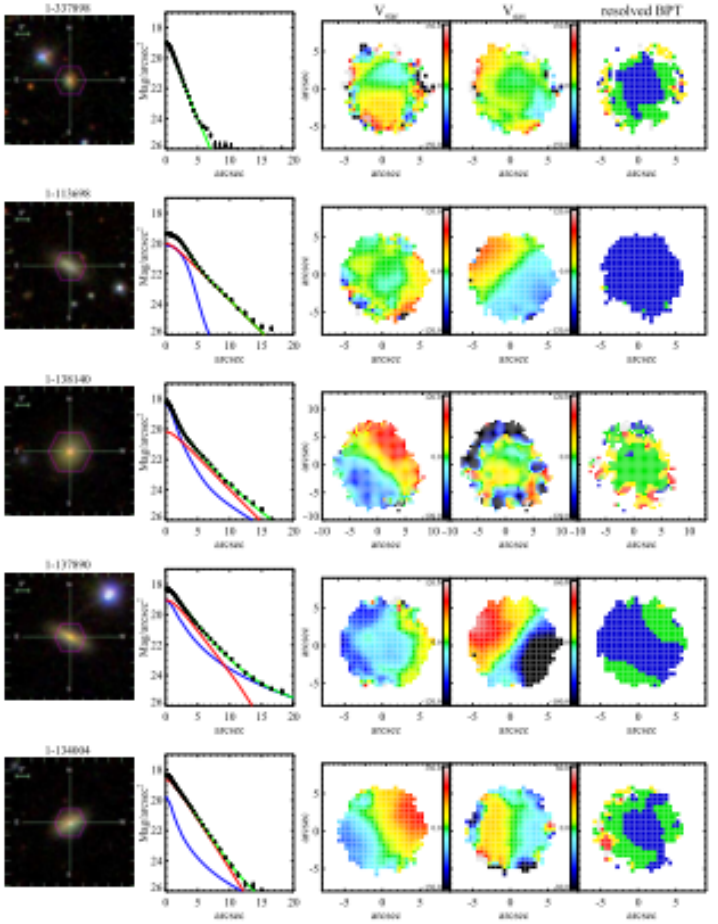

Figure 6: **Properties of the blue counter rotators.** Left: the SDSS false-color image; second column: the surface brightness profile, black is the data, green is the best fit model. Except for the first object, all the others are fitted by two components (red + blue); the third and fourth columns show the velocity fields of stars and gas, respectively. The velocities are in the unit of $\mathrm{km\ s^{-1}}$. The spatial resolved BPT diagram[31] is shown in the last column, blue represents star forming region, red represents Seyfert, green is the composite of AGN and star formation and yellow represents Low-Ionization Emission-line Region (LIER).

SDSS-IV MaNGA: Properties of galaxies with kinematically decoupled stellar and gaseous components

Yifei Jin[1,2,3], Yanmei Chen[1,2,3⋆], Yong Shi[1,2,3], C. A. Tremonti[4], M. A. Bershady[4], M. Merrifield[5], E. Emsellem[6,7], Hai Fu[8], D. Wake[4,9], K. Bundy[10], Lihwai Lin[11], M. Argudo-Fernandez[12,18], Song Huang[10], D. V. Stark[10], T. Storchi-Bergmann[13,22], D. Bizyaev[14,15], J. Brownstein[16], J. Chisholm[4], Qi Guo[17], Lei Hao[18], Jian Hu[19], Cheng Li[19], Ran Li[17], K. L. Masters[20], E. Malanushenko[14], Kaike Pan[14], R. A. Riffel[21,22], A. Roman-Lopes[23], A. Simmons[14], D. Thomas[20], Lan Wang[17], K. Westfall[21], and Renbin Yan[24]

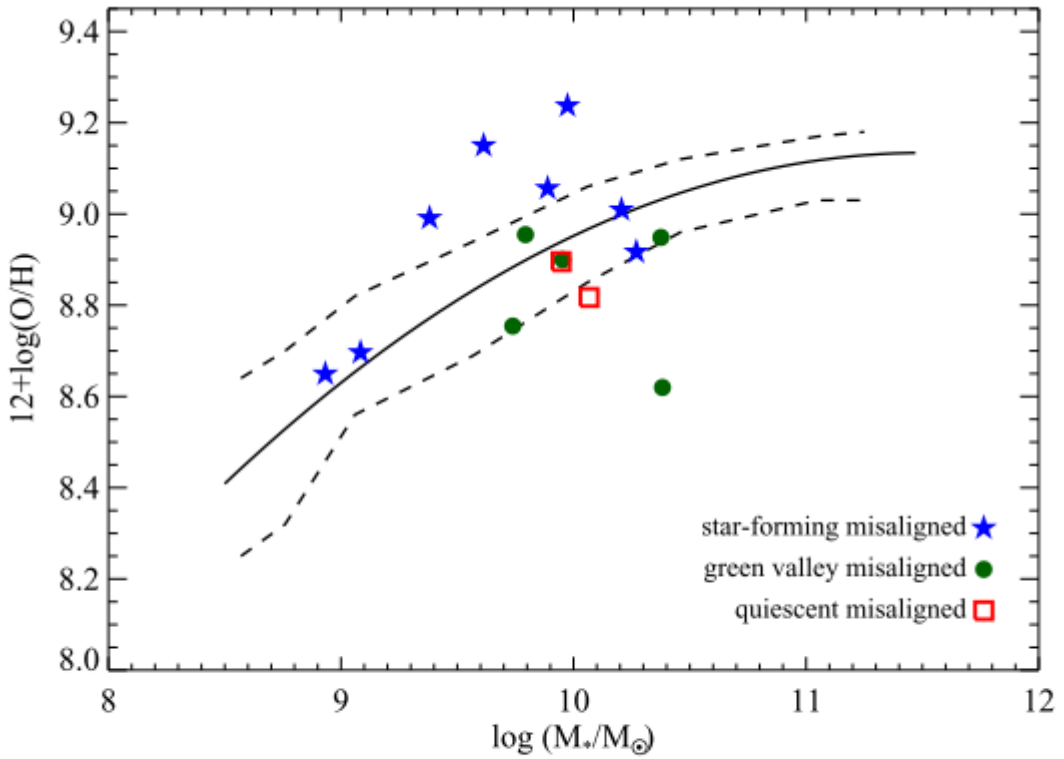

Figure 9. The stellar mass-metallicity relation. The solid line show the stellar mass-metallicity relation for the local star forming galaxies given by Tremonti et al. (2004). The two dashed lines show the $\pm 1\sigma$ scatter region. The color symbols show the 8 star-forming (blue star), 5 green valley (green dot) and 2 quiescent (red square) misaligned galaxies.

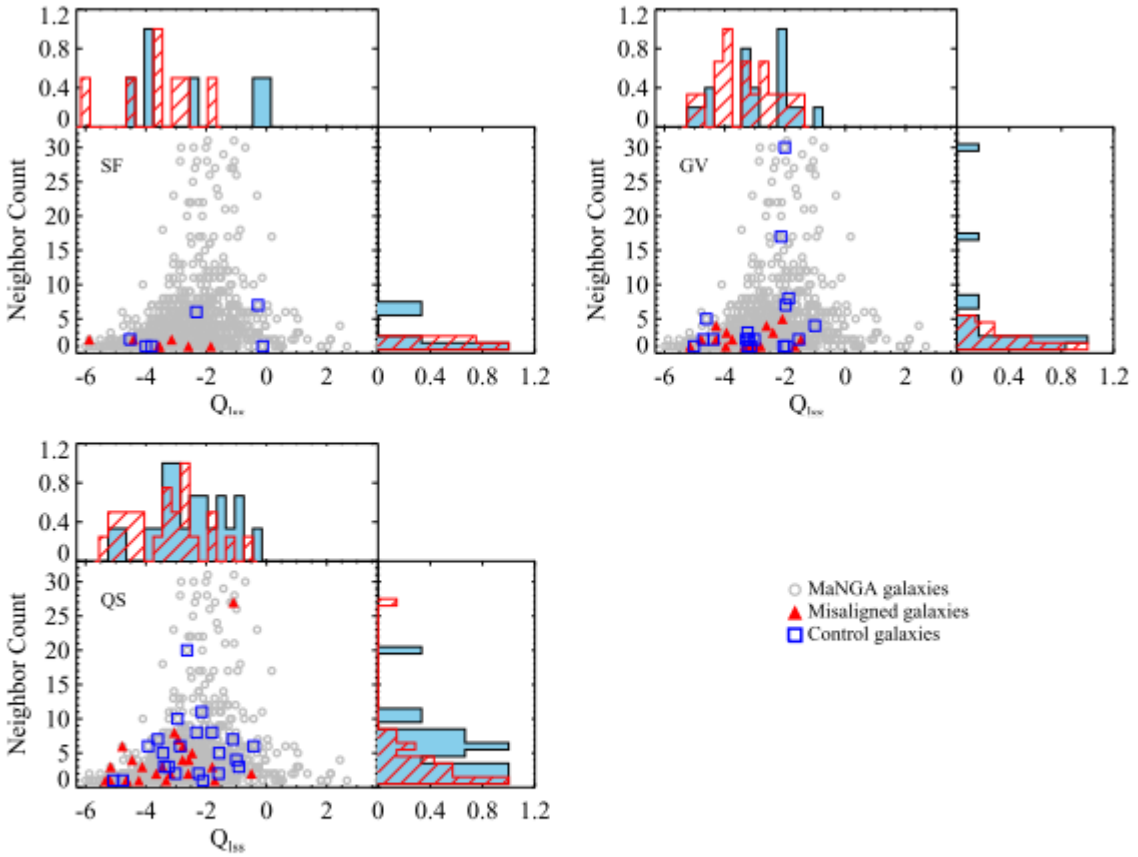

Figure 11. The Q_{lss} parameter versus neighbor counts diagrams. Three panels show the diagrams for star-forming, green valley and quiescent misaligned galaxies, respectively. In each panel, the grey open circles represent 1220 MaNGA galaxies. The kinematically misaligned galaxies and the control sample are presented as red triangles and blue squares, respectively. The top histogram gives Q_{lss} distribution and the right panel shows the distribution of neighbor counts. The histogram filled with red lines is for the kinematically misaligned sample and that filled with blue color is for the control sample. The peaks of all distributions are set to 1.